Rapid and Facile Formation of P3HT Organogels via Spin Coating: Tuning Functional Properties of Organic Electronic Thin Films

*Cameron S. Lee, Wen Yin, Adam P. Holt, Joshua R. Sangoro, Alexei P. Sokolov, and Mark D. Dadmun**

Poly(3-hexyl thiophene) (P3HT) is widely regarded as the benchmark polymer when studying the physics of conjugated polymers used in organic electronic devices. P3HT can self-assemble via π–π stacking of its backbone, leading to an assembly and growth of P3HT fibrils into 3D percolating organogels. These structures are capable of bridging the electrodes, providing multiple pathways for charge transport throughout the active layer. Here, a novel set of conditions is identified and discussed for P3HT organogel network formation via spin coating by monitoring the spin-coating process from various solvents. The development of organogel formation is detected by in situ static light scattering, which measures both the thinning rate by reflectance and structural development in the film via off-specular scattering during film formation. Optical microscopy and thermal annealing experiments provide ex situ confirmation of organogel fabrication. The role of solution characteristics, including solvent boiling point, P3HT solubility, and initial P3HT solution concentration on organogel formation, is examined to correlate these parameters to the rate of film formation, organogel-onset concentration, and overall network size. The correlation of film properties to the fabrication parameters is also analyzed within the context of the hole mobility and density-of-states measured by impedance spectroscopy.

1. Introduction

Low-bandgap conjugated polymers are suitable for a wide range of applications due to their potential benefits in low-cost, easy to manufacture electronic devices. Poly(3-hexylthiophene-2,5-diyl) (P3HT) has become a model conjugated polymer studied in this field due to its high hole mobility, solution processability, and potential to self-assemble during processing.[1] A particularly significant hurdle in the fabrication of devices using conjugated polymers is the need for a coherent understanding of the morphology, which dramatically impacts performance in organic field-effect transistors (OFETs), organic photovoltaics (OPVs), and related electronic devices.[2,3] Engineering an interconnected active layer that spans the length of the electrode is an overarching goal of designing an efficient electronic pathway in devices that utilize conjugated polymers.[1,4–6] Organogels, which consist of large percolating networks made up of clusters of polymer fibrils, offer an opportunity to realize these targeted morphologies, as they bridge electrodes and provide effective transport pathways throughout the active layer.

It has been shown that P3HT and other conjugated polymers can self-assemble in solution as semicrystalline fibers into 3D percolating networks that are up to micrometers in size due to π-stacking.[7–12] Films formed from these gelled networks can be used as flexible platforms in the design of organic electronic devices because they usually have much higher conductivities than comparable films generated under traditional conditions.[9,13] Understanding and tuning the self-assembly of conjugated polymer in these organogels, therefore, grants the opportunity to engineer these structures to directly benefit performance.

Previous studies have suggested that the self-assembly and resulting morphology of the gels are driven by the solution conditions (i.e., solvent, temperature, etc.).[14–17] Typically, these organogels are fabricated by aging and/or cooling the gels directly from solution, freeze-drying methods, emulsification in an aqueous solution, or sonication from homogeneous solutions.[9,18–20] Moreover, designing specific gel sizes requires an understanding of the driving forces that direct their self-assembly and the progression of intermediate structures during formation. Control of the unique formation conditions afforded by casting or formulation techniques can also provide controllable parameters that can guide the organogels to tunable structures.[14,21,22] When the polymer is in dilute solution,

C. S. Lee, Dr. W. Yin, Prof. A. P. Sokolov, Prof. M. D. Dadmun
Department of Chemistry
University of Tennessee
1420 Circle Dr. Knoxville, TN 37996-1600, USA
E-mail: dad@utk.edu
A. P. Holt
Department of Physics and Astronomy
University of Tennessee
1408 Circle Dr. Knoxville, TN 37996-1200, USA
Prof. J. R. Sangoro
Department of Chemical and Biomolecular Engineering
University of Tennessee
1512 Middle Drive Knoxville, TN 37996-2200, USA
Prof. A. P. Sokolov, Prof. M. D. Dadmun
Chemical Sciences Division
Oak Ridge National Laboratory
1 Bethel Valley Rd., Oak Ridge, TN 37831, USA

DOI: 10.1002/adfm.201501707

fibers grow individually or in discrete fiber bundles (i.e., colloidal networks) that form independent of solvent or concentration.[13,23–25] Malik first developed, and Pozzo further explored, a thermoreversible mechanism to form organogels by taking concentrated solutions (usually above 5 mg mL^{-1}, depending on solvent), cooling from 80 to 20 °C and aging over the span of several hours.[13,26,27] These networks feature fibrillar branching and roping, as well as observed growth from dense nucleation centers, which presumably originates due to impurities such as residual polymerization catalyst or high molecular weight fractions that may not fully dissolve.[13] These methods of gel growth are dictated by reducing solubility, leading to a nucleation-and-growth mechanism that produces gels in solution over a period of hours. This process allows the solution to reach a steady state structure after a long period of time.

Alternatively, the active layers in many organic electronic devices are often fabricated by spin coating, a nonequilibrium process. In spin coating, the solvent quickly evaporates leaving behind a concentrated polymer film in minutes. Moreover, spin coating can offer a facile fabrication method to realize organogel-based films if the proper conditions for their formation can be ascertained. In the spin-coating process, both thermodynamics and kinetics dictate the film formation process. The thermodynamics reflect the fundamental properties of the polymer solution from which the film is formed, including the Flory–Huggins interaction parameter, X, between the polymer and solvent, the composition of the initial solution, and the spin-coating parameters.[2] The kinetics of film formation is influenced by solvent choice, evaporation rate, crystallization behavior, and also postformation treatments such as thermal annealing (TA).[2,28]

The design and scope of the work reported herein is therefore to determine the conditions for the spin coating of P3HT that promote the growth of large organogels directly from a dissolved solution using spin coating. By means of a novel in situ static light scattering (SLS) instrument, the off-specular scattering of the film is monitored during the spin-coating process, which provides information on the structures that exist in the plane of the film during formation. This instrument also provides the thickness of the film during the spin-coating process via the specular reflectivity. With this information, the time and concentration that the film becomes solid is elucidated and the conditions for the formation of in-plane structures in the film during the spin-coating process are determined. This combination of structural information provides the foundation that can be used to tune the self-assembly and size of organogels that are formed during spin coating. Additionally, the structural characteristics of the formed organogels are correlated to relevant electronic properties to elucidate the impact of this level of structural control on performance of these films.

2. Light Scattering Results

The development of spin-coated films is characterized by two thinning regimes. Hydrodynamic thinning dominates thinning in the early stages of film formation, and later, evaporation is the predominant thinning mechanism.[29] Most of the solution is cast off in the initial seconds of spin coating, leaving behind a thin fluid layer on the substrate. This layer continues to decrease in thickness, first due to fluid flow and later by solvent evaporation.[30] The experiments completed here allow us to follow the latter evaporation-dominated regime. The specular reflectivity can be interpreted to determine both the rate of thinning and the time at which the film becomes solid. During spin coating, the reflectance produces a series of peaks and troughs as the film thins due to interference. With knowledge of the final thickness of the cast samples, which is measured using the atomic force microscopy scratch method, the time evolution of the thickness is constructed. This analysis utilizes Bragg's law

$$m\lambda = 2nD_t\cos\theta_i \quad (1)$$

for constructive interference. In this equation, n is the refractive index of the solution, θ_i is the incidence angle of the laser on the sample, D_t is the film thickness at time t, λ is the wavelength of the laser, and m is an integer. Therefore interference is a property of optical thickness, which is the product of film thickness and refractive index (n). The change in film thickness is determined from the position of the peak maxima (where there is complete constructive interference) and trough minima (where there is complete destructive interference) with respect to time, enabling construction of a thickness-time profile from the interference peaks. In this analysis, it is assumed that the refractive index changes linearly with time from the refractive index of the initial P3HT solution at time 0 to the refractive index of the final solid polymer film at the longest time in order to correct for the changing composition of the film with drying time. (Figure S1, Supporting Information) shows typical reflectance patterns for the film formed from a 3 wt% P3HT solution in bromobenzene (BB) (left) and the film formed from a 3 wt% P3HT solution in *o*-dichlorobenzene (ODCB) (right). The disappearance of the peaks in the reflectance patterns of Figure S1 (Supporting Information) mark the end of the thinning of the film by evaporation. Plots of the film thickness as a function of time that are derived from the reflectance patterns are presented in **Figure 1** for a variety of solutions. The rate of the thinning of a film is determined largely by the vapor pressure (and thus boiling point (BP)) of the solvent and by the polymer concentration of the solution. Solvents with lower vapor pressures (and higher BPs) evaporate more slowly, which increases the film formation time and a slowing of the thinning rate. For example, the 3 wt% P3HT solution in trichlorobenzene (TCB) (BP = 219–222 °C) requires the longest time for the film to form (≈323 s) and exhibits the slowest rate of thinning. On the other hand, Solutions of 2.5 and 3 wt% P3HT in ODCB (BP = 180.5 °C) and 2 and 3 wt% P3HT in BB (BP = 156 °C) take ≈70–100 and ≈30–35 s, respectively, exhibiting a faster rate of thinning than the TCB sample due to their lower BPs.

Additionally, for a given solvent, the concentration of polymer in the initial solution impacts the rate of the film formation. For example, the film from the 2.5 wt% P3HT solution in ODCB forms in 73 s, while the film from the 3 wt% P3HT solution in ODCB forms in 100 s. A small increase in the formation time is observed with an increase in P3HT concentration in all solvents, likely due to an increase in viscosity for the more concentrated samples. The solvents with the lowest BPs

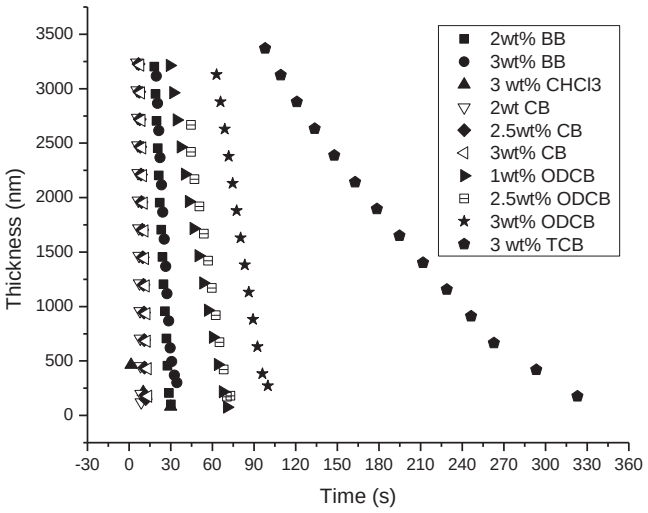

Figure 1. The thickness of the spin-coated P3HT films as a function of time during spin coating in various solvents and concentrations.

produce films the fastest, as evidenced by the formation of films from BB (BP = 156 °C) and chlorobenzene (CB) (BP = 131 °C), which produced in ≈30 and 15 s, respectively. This information therefore provides the foundation to quantitatively control the kinetics of the film-formation mechanism.

In addition to gathering information on the drying rate and time evolution of the film thickness, the in situ light scattering instrument monitors the development of structures in the plane of the film by analysis of the off-specular scattering of the film as a function of formation time. The length scales (l) that are monitored by the light scattering instrument are related to the scattering vector in reciprocal space, $\vec{q}$, such that

$$\vec{q} = \frac{4\pi \sin\theta}{\lambda} = \frac{4\pi \sin\left(\frac{1}{2}\arctan\left(\frac{r}{L}\right)\right)}{\lambda} \text{ and } l = 2\pi/|\vec{q}| \quad (2)$$

where λ is the wavelength of the laser, θ is the angle of the laser on the substrate, r is the radius of the pixel on the scattering screen, and L is the length from the sample to the screen. The setup is capable of detecting structures on the order of ≈2–12 µm. All samples produced scattering from structural changes occurring in the plane of the film, however, samples that exhibited peaks enabled structure information to be calculated from the position of the peak maxima in reciprocal space, $\vec{q}\max$. The emergence of such peaks indicates the formation of large 2D lateral structures with a dominant length scale present in the plane of the film. For samples that exhibited this peak, the off-specular scattering was radially symmetric and remained so throughout the film-formation process, indicating isotropic structures. The radially averaged scattering patterns of the samples containing peaks were analyzed to provide an average size of structures that emerged in the plane of the film during film formation.

A summary of the SLS experiments are presented in **Table 1**. Structures exhibiting a lateral peak from the final, dried film reductions produced structures with a dominant length scale between ≈3.2 and 8.7 µm, from the relation $l(2\pi/\vec{q}\max)$. Modification of the structure size and propensity to form such structures are governed by solubility, solution concentration, and boiling point of the solvent. The solvent boiling point provides the framework for the duration of formulation, and thus the rate at which the structures develop and emerge, as extrapolated from the thickness-time measurements. Additionally, the concentration and solubility of P3HT within a particular solvent creates environments that promote or hinder growth. Conditions that do not promote the lateral structures are designated as N/A in Table 1, demonstrating that multiple conditions are necessary to produce the observed SLS peaks. Correlation of the time dependence of the film formation to the evolution of the in-plane structures demonstrates that they begin to emerge at a given film thickness. The structures form during the thinning of the films in the later stages of the evaporation-dominated regime. During this part of the film formation process, the concentration of polymer is rapidly increasing, suggesting that the films must be sufficiently concentrated to form the in-plane structures.

To quantify this relationship, Equation (3) provides the relationship between the film thickness and solution concentration at any given time during the spin-coating process. In this equation, D_o is the measured final thickness of the film, ρ_{P3HT} is the density of P3HT, D_t is the thickness at time t during thinning, and ρ_s is the density of the solvent.

$$\text{P3HT}\frac{w}{w}\% = \frac{D_o \rho_{P3HT}}{D_o \rho_{P3HT} + (D_t - D_o)\rho_s} \cdot 100\% \quad (3)$$

Equation (3) allows us to determine the concentration of polymer in the film throughout the evaporative stage of formation. This can then be interpreted to provide insight into the role of the solution concentration and thermodynamics on the formation of the in-plane structures.

3. Discussion

The understanding of how polymer concentration and thickness changes throughout the evaporative phase of film formation during spin coating allows us to draw a correlation between the formation of structures in the plane of the film and the concentration of polymer in the film. This relationship for the films that are formed from CB, BB, and ODCB is shown in **Figure 2**. The shaded areas in Figure 2 designate the concentration regions where in-plane structures are detectable by SLS. The results from Figure 2 indicate that the ordered structures form in the final moments of the rapid evaporation in the film, and their formation depends on the solvent and the concentration of the initial solutions.

The concentration of polymer in the film when the in-plane structures begin to emerge varies significantly and appears to depend on the quality of the solvent. For instance, the concentration at which the in-plane structures first appear in the film formed from the 3 wt% P3HT solution in ODCB occurs ≈18–20 wt% P3HT, while the onset of in-plane structures in the film formed from the 3 wt% P3HT solution in BB occurs above ≈50 wt% P3HT. This difference can be correlated to the difference in the solubility of P3HT in these solvents, where

Table 1. Correlation of solvent and solution characteristics to film formation time and structure during spin coating.

Solvent	Polymer–solvent concentration [wt%]	Polymer concentration [mg mL^{-1}]	Solvent boiling point [°C]	P3HT solubility at RT[a)] [mg mL^{-1}]	Dominant length scale, *l* [μm]
$CHCl_3$	3.0	44.40	61.2	14.1	N/A
Tol	1.0	8.610	110	0.7	N/A
THT	3.0	29.97	119	37.6	4.7
THT	4.0	39.96	119	37.6	6.4
CB	2.5	27.75	131	15.9	3.2
CB	3.0	33.30	131	15.9	4.6
p-X	3.0	26.01	138.4	2.70	N/A
BB	2.0	29.90	156	84.1	3.3
BB	3.0	44.85	156	84.1	4.9
ODCB	2.5	32.50	180.5	14.7	4.7
ODCB	3.0	39.00	180.5	14.7	5.9
TCB	3.0	43.80	219–222	2.70	8.7

[a)]Taken from ref. [33].

P3HT has a lower solubility in ODCB (14.7 mg mL^{-1}) than in BB (84.1 mg mL^{-1}).[31] Moreover, CB has a P3HT solubility of 15.9 mg mL^{-1},[31] and the in-plane structures form at a similar concentration as ODCB, as in-plane structures emerge at ≈18 wt% P3HT. These observations are consistent with the aggregation, gelation, or precipitation of the P3HT from solution as the film becomes more concentrated being the dominant mechanism for the formation of the in-plane structure. The formation of the in-plane structures may, therefore, be due to the solution reaching a solubility limit during the evaporation driven by the relative increase in polymer concentration.

While the scattering clearly shows the presence of a structure with a dominant length scale, the identity of this structure is not directly known. Several possibilities exist for the identity of the structures, including the presence of droplets or pores that originate due to fluid flow or interfacial interactions during film thinning. Alternatively, dewetting of the film during processing could lead to droplet formation or originate from holes or pores formed in the film. The spontaneous spreading and dewetting for a drop of solution placed on a silicon substrate is characterized by the spreading coefficient *S*, which is related to the surface tensions between all of the interfaces.[32] For a film with $S < 0$,[33,34] annealing above its glass transition temperature ($T_g \gg 12.1$ °C for pure P3HT)[35] will result in dewetting of the film.

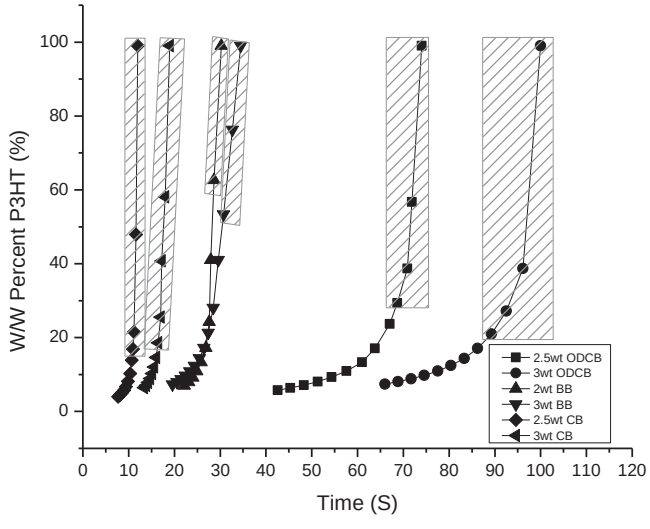

Figure 2. The P3HT concentration–time profile calculated from Equation (1) for samples of CB, BB, and ODCB during the later stages of film formation. The shaded regions correspond to the observance of ordered structures measured from the SLS setup. The results suggest that there is a solubility limit associated with the structure formation.

To investigate the possibility that the presence of pores or film dewetting is responsible for the observed in-plane structures, the P3HT films were exposed to a thermal annealing (TA) process for 30 min. The off-specular scattering pattern during thermal annealing monitors the change in the in-plane structures. The response to thermal annealing of two representative samples is shown in **Figure 3**, where these results show an increase in the peak intensity of the in-plane scattering peak with no change in the $\vec{q}$ max position with thermal annealing. Additionally, the peak position and intensity for the ODCB sample remained unchanged after 5 min, while the BB sample remained unchanged after 20 min of exposure to the TA process. Thus, the structures are retained with thermal annealing in the films formed from both the 3 wt% P3HT in BB and the 3 wt% P3HT in ODCB solutions. The retention of the in-plane structure with thermal annealing is counter to that which would be expected if the in-plane structure were the result of the formation of pores or from dewetting of the film, where structures caused by dewetting would grow with thermal annealing, shifting the peak maximum, q_{max}, to a smaller value. Similarly, if pores that were produced from the solvent flow during film formation were present, thermal annealing would cause the collapse of the pores, which would result in the shift and disappearance of the scattering peak maximum. Rather, the increase in scattering intensity with thermal annealing is consistent with the evaporation of residual solvent in a P3HT

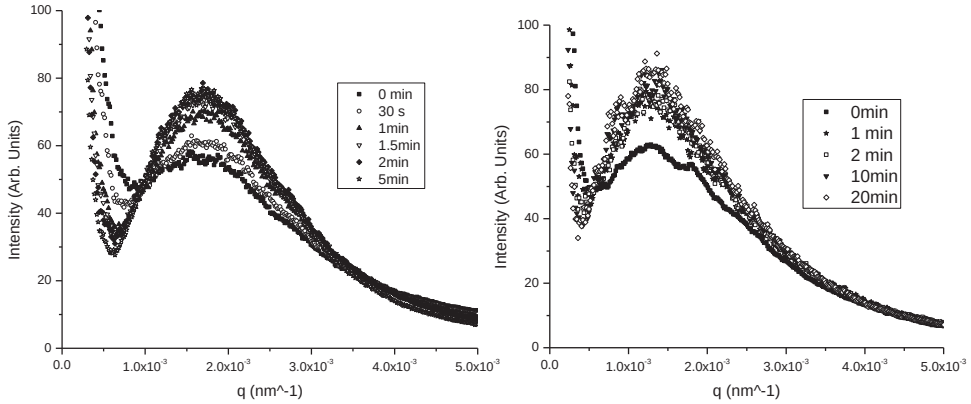

Figure 3. In plane scattering patterns of a film that is formed from 3 wt% ODCB (left) and 3 wt% BB (right) as a function of annealing time at 150 °C. These results reveal a coarsening of the structures.

aggregate, which creates greater contrast between the fibril and its surroundings.

Therefore, the structures that are observed by scattering are ascribed to organogel formation. P3HT has demonstrated the ability to form organogels from a number of solutions and conditions.[9,27,36] The π–π stacking of the P3HT backbone in solution leads to long nanowires that are up to micrometers in length, and the agglomeration and aggregation of these individual fibrils leads to an increase of hierarchical order into clusters or organogels. The fibrils form in the deposited solution, both growing and diffusing throughout the spin-coating process as the film dries. In the final phase of film formation, the concentration of P3HT in the film is increasing, promoting entanglement of the growing and diffusing fibrils. Additionally, the formation of organogels is consistent with the dependence of the formation time and size of the structure on the solubility of P3HT in a given solvent, as shown in Figure 2.

To provide further evidence for the formation of organogels, the films were spin cast onto glass substrates under identical conditions and observed with optical microscopy (OM). An optical image of the film formed from a 3 wt% P3HT solution in BB is shown in **Figure 4**, and is representative of the microscopic pictures of all films that produce a peak in the in-plane scattering in the thin films. These images verify the formation of micrometer-sized fibrils that are consistent with organogel formation.

Image analysis further quantifies the domain spacing of the structures in the image, where the domain spacings are determined from a profile plot. For the film formed from a P3HT solution in BB shown in Figure 4, the calculated domain spacing is ≈5.3 µm, with additional samples producing structures with domain sizes on the same order of magnitude. The fast Fourier transform (FFT) of the microscopy image of the film formed from a 3 wt% P3HT solution in BB is further analyzed by fitting the peak in the FFT to a Gaussian (Figure 4, bottom right). This analysis indicates that the dominant length scale in this image is ≈3.8 µm. The domain spacing that is obtained by analysis of the direct image, ≈5.3 µm and the dominant length scale that emerges from the analysis of the FFT of that image, ≈3.8 µm, both correspond well to the dominant length scale of 4.9 µm that is the result of the SLS experiment (see Table 1), verifying that the fibrils observed by optical microscopy are the objects that produce the peaks in the in situ light scattering experiments. Thus, the analysis of the range of experimental results presented here are consistent with the formation of organogels in P3HT thin films formed by spin coating.

3.1. Organogel Formation Conditions

With the identity of organogels verified, conditions that promoted organogel formation in P3HT films were further explored. These results demonstrate that solvent choice and solution concentration govern organogel formation and growth. **Figure 5** is a plot that correlates the initial solution concentration and the solvent boiling point conditions to the success of the formation of organogels. In this figure, the solid symbols indicate conditions that do not produce an organogel, open symbols correspond to conditions that do produce organogels after the film is completely dried, and the half-filled symbol refers to conditions that form a transient organogel that emerges during film formation but is lost in the final film.

It appears that the limited solubility of P3HT in some solvents, including *p*-xylene and toluene (2.7 and 0.7 mg mL^{-1}, respectively),[31] produce films that are too aggregated and nonuniform to create organogels during spin coating. All conditions that result in the formation of organogel structures in the final film require an initial solution concentration above ≈25 mg mL^{-1} in a solvent with a BP ≥ 119 °C. If the initial solution is below a concentration of 25 mg mL^{-1}, the number of fibrils is not sufficient for large-scale aggregation and growth. Additionally, if the initial solution is in a solvent with a BP < 119 °C, it appears that the film develops too quickly to allow the necessary aggregation/nucleation of the organogel to occur.

Therefore, these results indicate that organogel formation via spin coating requires the correct range of concentration and solubility (i.e., thermodynamic properties) as well as appropriate drying kinetics of film formation, which is related to solvent BP, to allow the agglomeration of P3HT into fibrillar networks during the deposition process. The lack of either condition results in the exclusion of this hierarchical aggregation process. For example, films formed from solution in $CHCl_3$, which provides sufficient P3HT solubility

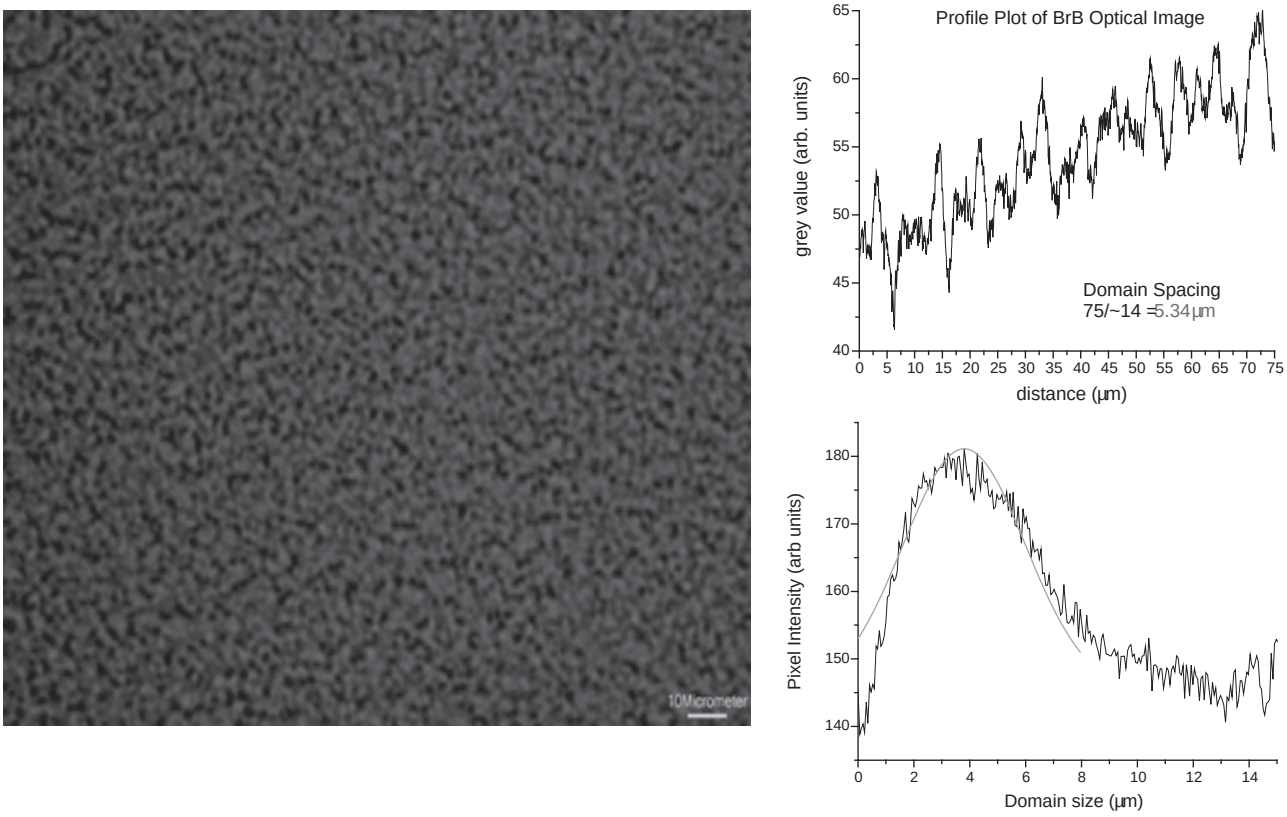

Figure 4. Optical image of the film formed from a 3 wt% P3HT solution in BB (left) (scale bar 10 mm). Image analysis produces domain spacing information (top right) by a density scan and a dominant domain size (bottom right) by analysis of the FFT of the image.

(14.1 mg mL^{-1}),[31] form too quickly due to its low BP (BP = 61.2 °C) to allow P3HT aggregation and organogel formation. Films formed from solutions of P3HT in BB, ODCB, tetrahydrothiophene (THT), TCB, and CB all possess the necessary solubility to create solutions and have a sufficiently high BP, and thus form organogels during this deposition process. In the special case of the 2 wt% P3HT solution in ODCB, the organogel appears to form during film formation, but is lost in the final film. This behavior can be explained as the system borders the concentration threshold of organogel formation, first experiencing gel growth near the surface during film formation due to a buildup of polymer concentration there, then the structure breaks up or redissolves as the solvent evaporates through the film.

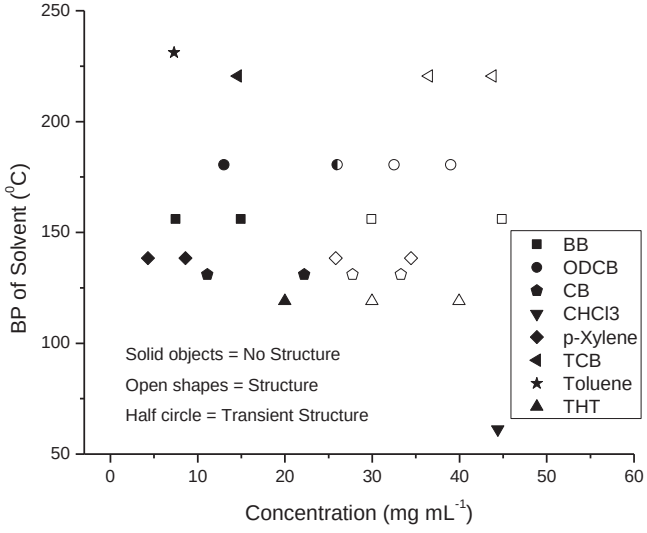

Figure 5. Correlation of organogel formation to solution concentration and boiling point of solvent. solid shapes denote conditions that form organogels, open shapes do not produce organogels, and the half-filled shape produces a transient structure. Initial concentrations above 25 mg mL^{-1} in solvents with BPs ≥ 119 °C provide the necessary conditions for organogel formation when spin cast at 1000 rpm.

3.2. Control of Organogel Characteristics

With knowledge of the organogel formation conditions, the impact of solution concentration on the characteristics of the ultimate organogel can be ascertained. (Figure S2, Supporting Information) summarizes the change in the scattering patterns of the final film with solution concentration for several solvents. These plots show that the peak in the scattering curve shifts to a smaller q_{max} with an increase in concentration, indicating an increase in the dominant size of the final organogel. In addition, the scattering peak becomes more defined with an increase in concentration, indicating a smaller distribution of sizes. The growth in size is likely due to the greater abundance of P3HT fibrils diffusing and entangling throughout the thinning of the film at the higher concentration.

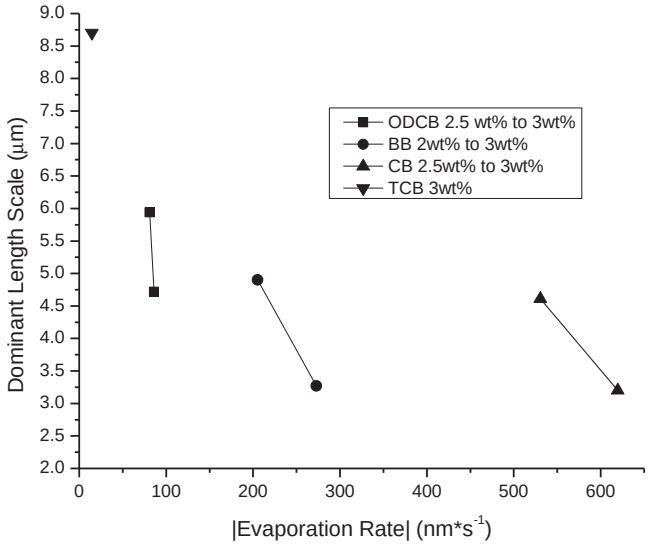

Figure 6. The dominant length scale of the organogel formed during spin coating as a function of the initial solution concentration and evaporation rate of the solvent during film formation.

Additionally, the choice of solvent and thus drying rates of the film affects the dominant size of the organogel. **Figure 6** demonstrates the effect of evaporation rate on the dominant size of the organogels and the values are summarized in **Table 2**. The boiling points for the solvents shown in Figure 6 are TCB > ODCB > BB > CB. The solvent with the highest BP (i.e., TCB) forms the largest organogels, on the order of ≈8.7 mm, as this film takes the longest to form the final film. Films produced from lower BP solvents exhibit smaller structures than the TCB sample, in part due to the shorter film formation time, which limits the growth of the organogel. The slopes of the lines that follow the organogel structure in the CB and BB samples are similar because the formation times of the films (12.0; 13.7, and 30.2 s; 34.5 s, respectively) do not vary much with initial solution concentration for these solvents. The slope of the ODCB samples, however, is approximately five times greater than that of the CB and BB samples, presumably due to the larger difference in formation time between the two concentrations (73.0 s for the 2.5 wt% sample and 100 s for the 3 wt% sample).

These results can be interpreted to show that an increase in P3HT concentration augments the number of fibril networks and growth centers that are formed during the early stages of spin coating. At longer formation times (i.e., for slower evaporation rates), increased growth time and agglomeration of fibrils lead to larger gel structures. As the polymer reaches its solubility limit during thinning, more and more P3HT fibrils emerge, precipitating out earlier in solvents with lower solubilities. This is demonstrated in the case of the film formed from the 3 wt% P3HT in TCB, which has a high BP (219–222 °C) and a low solubility (2.7 mg mL^{-1}), promoting conditions that produce the largest overall structures.

Table 2. Relationship between solution composition, domain size of the organogels, and evaporation rate.

Solvent	Polymer–solvent composition [wt%]	Polymer concentration [mg mL^{-1}]	Dominant length scale, *l* [mm]	|Evaporation rate| [nm s^{-1}]
CB	2.5	27.75	3.2	620
CB	3.0	33.30	4.6	530
BB	2.0	29.90	3.3	273
BB	3.0	44.85	4.9	205
ODCB	2.5	32.50	4.7	86.0
ODCB	3.0	39.00	5.9	81.0
TCB	3.0	43.80	8.7	14.5

3.3. Correlation of Organogel Formation to Electronic Performance

The formation of large organogel networks offers the opportunity to create improved pathways for charge transport throughout the active layer. Charge transport within such a network is expected to be faster than internetwork transport that occurs between adjoining fibers, where larger, more direct networks will promote improved hole mobility.[3,23,24] Hole mobility and density-of-states (DOS) are dependent on the multiscale morphology of the organogel, and thus the performance of the organogel networks formed during spin coating are characterized by impedance spectroscopy to evaluate the promise of this fabrication procedure to form viable organic electronics.

The samples that are examined by impedance spectroscopy were prepared by spin coating onto doped silicon wafers then placing gold-plated brass electrodes atop the sample in a parallel plate capacitor configuration. Impedance spectroscopy collected conductivity and capacitance information. The hole mobility of the p-doped[37–39] samples were determined from the transition of the samples from D.C. conductivity to A.C. conductivity. The results of this analysis are presented in **Figure 7**, which shows the hole hopping times of the examined organogels. The results indicate that an increase in domain size for a given solvent leads to a slower hole hopping process in the samples formed from solutions in ODCB (2.5 and 3 wt%), CB (2.5 and 3 wt%), and BB (2 and 3 wt%). These results also suggest that different hopping processes occur in the samples produced from different solvents, even considering variation in the size of the organogel. This indicates that the domain size is not the only parameter that controls the charge transport, but the assembly of the domains is crucially important as well. This is consistent with previous work that has shown that solvent choice impacts the nature of fibril assembly and its structural characteristics, such as length and density of the fibers, emphasizing that domain size alone does not control hole mobility.[23]

This can be observed in the data that show the organogel formed from P3HT solutions in ODCB possesses the fastest hole hopping times, on the order of 1.2×10^{-7} to 5.7×10^{-8} s, while the organogels formed from BB have the slowest hole hopping times, 1.2×10^{-5} and 7.4×10^{-6} s. Also, the organogels formed from ODCB undergo the longest drying process, which could account for the better transport properties due to increased local ordering and/or crystallinity. While the solubility of P3HT in CB is similar to that in ODCB, the shorter

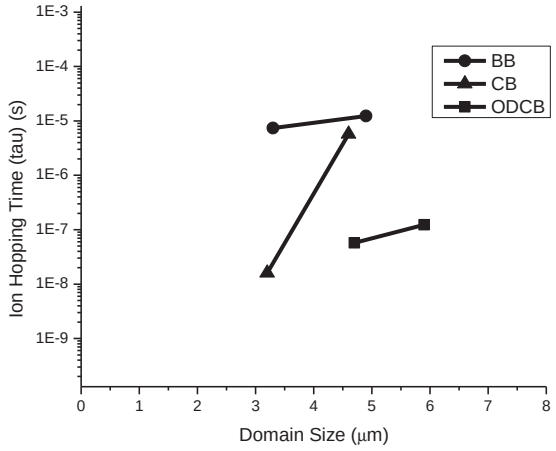

Figure 7. Hole hopping times as determined from impedance measurements. The higher initial concentrations of P3HT promote larger networks, which translate to slower hole transport.

film formation time appears to create an organogel that limits the hole hopping times relative to that of the organogels that are formed from ODCB to between 5.7×10^{-6} and 1.6×10^{-7} s. The higher solubility of BB appears to inhibit the extent of crystal and fiber growth, leading to slower transport properties despite the larger organogel domains.

Hole mobility depends not only on the local ordering of the P3HT, but also on the path that the hole can travel throughout the network. In semicrystalline polymers, it is assumed that hole transport primarily occurs in the ordered regions, while defects, grain-boundaries, and disordered regions all contribute to the number of localized states present at a given energy level.[40] The hole hopping times suggest that disordered regions are more prevalent in the organogels formed from higher concentrations. At the larger, network length scale, the organogels are made up of individual fibers that intersect at disordered junctions, and the resulting hole transport depends on the nature of the fibril overlaps in these junctions. For example, Pozzo et al. described junctions of fibers as either beneficial to hole mobility (i.e., bifurcations or simple contacts) or detrimental to hole mobility (i.e., fibril overlaps), the latter of which is more common.[23] Additionally, Samitsu et al. reported that isolated individual P3HT nanofibers display a higher hole mobility than P3HT networks due to the presence of fibrillar overlaps in the networks.[41] The hole hopping times of the samples presented in Figure 7 all reflect a retardation of hopping times with an increase in polymer concentration. Presumably, as the initial concentration of P3HT increases, the number of fibers increases, which promotes additional junctions and overlaps between fibers effectively decreasing the hole mobility of the film. These results therefore suggest that both domain size and organogel formation time are crucial parameters that impact the hierarchical ordering of the P3HT organogel and both must be considered when designing a fabrication procedure that will optimize electronic performance. These results further indicate that higher boiling solvents with modest solubility provide the best hierarchical polymer ordering in the resultant organogel for improved hole mobility.

Estimates of the DOS of the samples provide additional insight into the structure–performance relationship. The DOS determine the electrical potential as well as the role of defect states as trapping or recombination centers, which are inherently detrimental to performance. The DOS were analyzed by fitting a Gaussian shape centered at the maximum of the distribution E_0. The results, presented in **Figure 8**, reflect the number of electrons that exist at a given energy as well as defining the Fermi–Dirac distribution of electrons in the highest occupied molecular orbital (HOMO) levels of the film. The individual band broadening is due to the delocalization of π–π bands, resulting in the broad feature which spreads over 0.15 eV, and the sharper peaks ranging from 0.46 to 0.70 eV are attributed to a localized P3HT π–π band.[42] The disorder parameter, σ, which accounts for the broadening of the Gaussian DOS, lies within the range of 24–30 meV for the samples, in good agreement with values found in most cases for conducting polymers.[43,44]

Analysis of the DOS demonstrates the contribution of the gel and crystalline morphology to device characteristics. A larger number of electronic states exist in films formed from the lower initial P3HT concentrations. The DOS of the organogel resulting from 2.5 wt% P3HT in ODCB is $\approx 30 \times 10^{16}$ eV cm^{-3}, while the organogel resulting from 3 wt% P3HT in ODCB has a DOS that is six times lower, $\approx 5 \times 10^{16}$ eV cm^{-3}. Similarly in the organogels formed from CB, the 2 wt% sample has a DOSv of $\approx 8.5 \times 10^{16}$ eV cm^{-3}, while the 3 wt% has a DOS that is four times lower with a value of $\approx 2 \times 10^{16}$ eV cm^{-3}. A larger density of charge correlates to a more favorable orientation and path of P3HT molecules in the film.

The presence of grain boundaries and disordered regions originating from fibril overlaps or other intrinsic impurities that arise during film fabrication, such as molecular orientation, vacancies, dangling bonds, or chain ends often lead to the defects observed in the vacuum level bending and resulting HOMO level offset with impedance measurements.[45,46] P3HT organogel OFETs can exhibit HOMO-level band bending at the metal–polymer interface junction, creating a depletion zone at the cathode contact, known as Schottky-diode behavior.[47,48] Charged defects within the gap alter the electric field profile

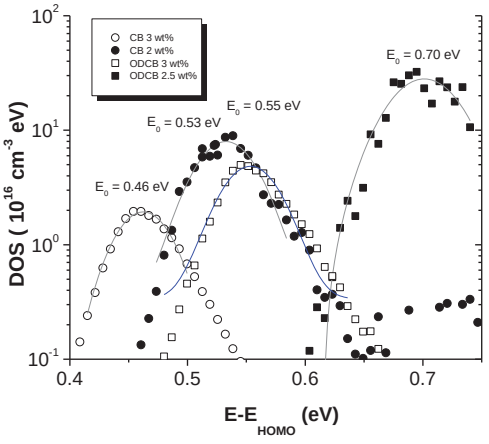

Figure 8. Density of states of spin-cast samples as a function of the energy with respect to the P3HT HOMO level. Gaussian fits are also displayed.

and reduces the drift driving force for carrier transport and consequently diminishes carrier collection at the contacts.[46] The organogel films formed from higher concentration samples of P3HT promote more charge injection, likely due to the presence of more disordered regions, leading to Fermi level bending toward that of the cathode. For example, the E_0 of the organogel formed from 2.5 wt% P3HT in ODCB is 0.70 eV while the larger organogel formed from 3 wt% P3HT is 0.55 eV. Similarly, the E_0 of the organogel formed from the 2 wt% solution in CB is 0.53 eV, while that of the organogel formed from the 3 wt% solution is 0.46 eV. The extent of band bending, i.e., alteration of the vacuum level toward the cathode, is dependent upon the chemical potential gradient that exists at the film–cathode interface, and is strongly influenced by the crystallinity and morphology of the P3HT film.[49] Thus, the DOS data are consistent with the hole hopping times, suggesting that the larger domains that are formed from higher concentrations appear to have more defects that limit charge transport. Similarly, the reported hole hopping times provide direct insight into the role of solvent boiling point and solubility on the hierarchical polymer ordering in, and electronic performance of, the resultant organogel.

4. Conclusions

We demonstrate the ability to create P3HT organogels via spin coating. Moreover, the results offer parameters that can be modified to tune organogel formation directly from dissolved solutions of P3HT from a number of common solvents used in the fabrication of organic electronics. Static light scattering experiments determine that a minimum P3HT concentration of 25 mg mL^{-1} and a solvent BP at or above 119 °C are required for organogel formation. By adjusting solution conditions that promote structure growth, organogels with average domain sizes from ≈3.3 to 8.7 μm are produced. Additionally, the concentrations of P3HT in solution at which the structures begin to emerge during the thinning of the film are determined from the thickness-time profiles and correlated to the solubility and boiling point of the solvent used. The average domain sizes of the gels are dependent on P3HT concentration and film-formation time, which highlight the duality of kinetics and thermodynamics to the structure evolution and morphology of spin-coated films. Experimentally derived hole-hopping times are found to exhibit an inverse relationship with the average domain sizes, which is consistent with an increase in disordered domains. Additionally, samples with a lower initial concentration exhibit lower ionization potentials and larger DOS at the maximum energy. These results indicate the complexity of the 3D percolating networks and that structural considerations must be taken into account when incorporating organogels into devices.

5. Experimental Section

Regioregular poly(3-hexylthiophene-2,5-diyl) (P3HT) solutions were prepared by adding 1–3 wt% P3HT to ODCB, CB, TCB, chloroform ($CHCl_3$), BB, toluene (tol), *p*-xylene (p-x), or THT. The polymer, Sepiolid P200 poly(3-hexylthiophene-2,5-diyl) (Lot#A6-7), was purchased from Reike Metals (Lincoln, NE) and used as received. The manufacturer's reported molecular weight is <50 000 g/mol with a polydispersity index (PDI) = 2.0. The regioregularity was reported by the manufacturer to be ≥95%. Solutions were prepared by heating to 80 °C for 4 h until the polymer was fully dissolved. The polymer was considered dissolved when the solution appeared bright orange and no visible sign of solids remained. The dissolved solutions were deposited onto an ≈3 cm^2 silicon substrate placed atop a spin-coater chuck and promptly spun at 1000 rpm for 3–7 min until a solid film is formed.

To monitor the structural changes that exist in the film during formation, the light from a laser was positioned at the center of the deposited sample on the substrate. Laser measurements were performed using a Research Electro-Optics, Inc. helium–neon laser (632.8 nm) with a power of 5.0 mW. The incident angle of the laser was 35° to the normal of the sample. The laser light that is scattered or reflected from the film was collected by two detectors simultaneously—a photodiode for reflectivity, and a paper screen and charge-coupled-device camera for off-specular scattering. The apparatus is based on a previously reported instrument[50,51] and is adapted to a q-range to detect relevant structures in our films. TA was performed under the same instrument configuration, except the spin coater is replaced with a hot plate that is set to 150 °C for 30 min. The final films were also examined by OM using an Olympus BH-2 Series microscope at a magnification of 40× with phase-contrasting objectives. The films were fabricated by spin coating on glass substrates under identical conditions as the scattering experiments for visibility by OM. The images of the final films from optical microscopy were analyzed with Image-J software. Broadband impedance spectroscopy measurements were performed with an impedance analyzer from Novocontrol (Alpha analyzer) in the frequency range of 10^{-1}–10^{7} Hz and an A.C. voltage of 0.1 V. The measurements were carried out in a custom-made sample cell at room temperature and under dry nitrogen. The samples were prepared in a parallel plate configuration where the P3HT films were spin coated on highly n-doped silicon wafers and then capped with n-doped silicon wafers covered with 260 nm nanostructured silica spacers.

Supporting Information

Supporting Information is available from the Wiley Online Library or from the author.

Acknowledgements

The authors wish to acknowledge the Sustainable Energy Education Research Center and support from TN-SCORE, a multidisciplinary research program sponsored by NSF-EPSCOR (EPS-1004083). A.P.H. and A.P.S. acknowledge financial support of the Department of Energy, Office of Basic Energy Sciences, Division of Materials Sciences and Engineering.

Received: April 27, 2015
Revised: July 16, 2015
Published online: August 18, 2015

[1] X. Yang, J. Loos, S. C. Veenstra, W. J. H. Verhees, M. M. Wienk, J. M. Kroon, M. A. J. Michels, R. A. J. Janssen, *Nano Lett.* **2005**, *5*, 579.
[2] X. Yang, J. Loos, *Macromolecules* **2007**, *40*, 1353.
[3] M. T. Dang, L. Hirsch, G. Wantz, J. D. Wuest, *Chem. Rev.* **2013**, *113*, 3734.

[4] J. Halls, C. Walsh, N. Greenham, *Nature* **1995**, *376*, 498.
[5] G. Yu, J. Gao, J. Hummelen, F. Wudl, A. J. Heegert, *Science* **1995**, *270*, 1789.
[6] G. Yu, A. J. Heeger, *J. Appl. Phys.* **1995**, *78*, 4510.
[7] D. Alcazar, F. Wang, T. M. Swager, E. L. Thomas, *Macromolecules* **2008**, *41*, 9863.
[8] C. C. Kitts, D. A. Vanden Bout, *Polymer* **2007**, *48*, 2322.
[9] S. Malik, T. Jana, A. K. Nandi, *Macromolecules* **2001**, *34*, 275.
[10] S. Malik, A. K. Nandi, *J. Polym. Sci., Part B: Polym. Phys.* **2002**, *40*, 2073.
[11] S. Malik, A. K. Nandi, *J. Phys. Chem. B* **2004**, *108*, 597.
[12] P.-S. Wang, H.-H. Lu, C.-Y. Liu, S.-A. Chen, *Macromolecules* **2008**, *41*, 6500.
[13] G. Newbloom, K. Weigandt, D. Pozzo, *Macromolecules* **2012**, 45, 3452.
[14] J.-L. Li, B. Yuan, X.-Y. Liu, H.-Y. Xu, *Cryst. Growth Des.* **2010**, *10*, 2699.
[15] X. Y. Liu, P. D. Sawant, *Adv. Mater.* **2002**, *14*, 421.
[16] P. Terech, R. G. Weiss, *Chem. Rev.* **1997**, *97*, 3133.
[17] V. Percec, C.-H. Ahn, G. Ungar, D. J. P. Yeardley, M. Moller, S. S. Sheiko, *Nature* **1998**, *391*, 161.
[18] P.-T. Huang, Y.-S. Chang, C.-W. Chou, *J. Appl. Polym. Sci.* **2011**, *122*, 233.
[19] B.-G. Kim, E. J. Jeong, H. J. Park, D. Bilby, L. J. Guo, J. Kim, *ACS Appl. Mater. Interfaces* **2011**, *3*, 674.
[20] J. J. Richards, K. M. Weigandt, D. C. Pozzo, *J. Colloid Interface Sci.* **2011**, *364*, 341.
[21] P. Terech, R. G. Weiss, *Chem. Rev.* **1997**, *97*, 3133.
[22] S. Zhang, D. M. Marini, W. Hwang, S. Santoso, *Curr. Opin. Chem. Biol.* **2002**, *6*, 865.
[23] G. M. Newbloom, F. S. Kim, S. A. Jenekhe, D. C. Pozzo, *Macromolecules* **2011**, *44*, 3801.
[24] S. Berson, R. De Bettignies, S. Bailly, S. Guillerez, *Adv. Funct. Mater.* **2007**, *17*, 1377.
[25] S. Samitsu, T. Shimomura, K. Ito, *Thin Solid Films* **2008**, *516*, 2478.
[26] S. Malik, A. K. Nandi, *J. Appl. Polym. Sci.* **2007**, *103*, 2528.
[27] G. M. Newbloom, K. M. Weigandt, D. C. Pozzo, *Soft Matter* **2012**, *8*, 8854.
[28] H. Hoppe, N. S. Sariciftci, *J. Mater. Chem.* **2006**, *16*, 45.
[29] P. Mokarian-Tabari, M. Geoghegan, J. R. Howse, S. Y. Heriot, R. L. Thompson, R. A. L. Jones, *Eur. Phys. J. E: Soft Matter* **2010**, *33*, 283.
[30] A. G. Emslie, F. T. Bonner, L. G. Peck, *J. Appl. Phys.* **1958**, *29*, 858.
[31] F. Machui, S. Langner, X. Zhu, S. Abbott, C. J. Brabec, *Sol. Energy Mater. Sol. Cells* **2012**, *100*, 138.
[32] M. J. Rosen, *Surfactants and Interfacial Phenomena*, 3rd ed., Wiley-Interscience, Hoboken, NJ **2004**.
[33] F. Leroux, C. Campagne, A. Perwuelz, L. Gengembre, *J. Colloid Interface Sci.* **2008**, *328*, 412.
[34] I. Karapanagiotis, W. W. Gerberich, *Surf. Sci.* **2005**, *594*, 192.
[35] J. Zhao, A. Swinnen, G. Van Assche, J. Manca, D. Vanderzande, B. Van Mele, *J. Phys. Chem. B* **2009**, *113*, 1587.
[36] W. Xu, H. Tang, H. Lv, J. Li, X. Zhao, H. Li, N. Wang, X. Yang, *Soft Matter* **2012**, *8*, 726.
[37] M. S. A. Abdou, F. P. Orfino, Y. Son, S. Holdcroft, *J. Am. Chem. Soc.* **1997**, *119*, 4518.
[38] S. Hoshino, M. Yoshida, S. Uemura, T. Kodzasa, N. Takada, T. Kamata, K. Yase, *J. Appl. Phys.* **2004**, *95*, 5088.
[39] E. J. Meijer, A. V. G. Mangnus, B.-H. Huisman, G. W. 't Hooft, D. M. de Leeuw, T. M. Klapwijk, *Synth. Met.* **2004**, *142*, 53.
[40] A. Salleo, *Mater. Today* **2007**, *10*, 38.
[41] S. Samitsu, T. Shimomura, S. Heike, T. Hashizume, K. Ito, *Macromolecules* **2010**, *43*, 7891.
[42] W. R. Salaneck, O. Inganäs, B. Thémans, J. O. Nilsson, B. Sjögren, J.-E. Österholm, J. L. Brédas, S. Svensson, *J. Chem. Phys.* **1988**, *89*, 4613.
[43] J. Bisquert, G. Garcia-Belmonte, J. García-Cañadas, *J. Chem. Phys.* **2004**, *120*, 6726.
[44] I. N. Hulea, H. B. Brom, A. J. Houtepen, D. Vanmaekelbergh, J. J. Kelly, E. A. Meulenkamp, *Phys. Rev. Lett.* **2004**, *93*, 166601.
[45] N. Koch, *Phys. Status Solidi RRL* **2012**, *6*, 277.
[46] P. P. Boix, G. Garcia-Belmonte, U. Muñecas, M. Neophytou, C. Waldauf, R. Pacios, *Appl. Phys. Lett.* **2009**, *95*, 233302.
[47] G. Dennler, C. Lungenschmied, N. S. Sariciftci, R. Schwödiauer, S. Bauer, H. Reiss, *Appl. Phys. Lett.* **2005**, *87, 163501*.
[48] G. Garcia-Belmonte, A. Munar, E. M. Barea, J. Bisquert, I. Ugarte, R. Pacios, *Org. Electron.* **2008**, *9*, 847.
[49] F. E. Osterloh, M. A. Holmes, L. Chang, A. J. Moulé, J. Zhao, *J. Phys. Chem. C* **2013**, *117*, 26905.
[50] S. Y. Heriot, R. A. L. Jones, *Nat. Mater.* **2005**, *4*, 782.
[51] P. C. Jukes, S. Y. Heriot, J. S. Sharp, R. A. L. Jones, *Macromolecules* **2005**, *38*, 2030.